Experimental Investigation of a Supersonic Shear Layer with Slot Injection of Helium

F. T. Kwok,* P. L. Andrew,† W. F. Ng,‡ and J. A. Schetz§
Virginia Polytechnic Institute and State University, Blacksburg, Virginia 24061

This study focuses on mixing in a shear layer developed from helium slot injection into a parallel supersonic airstream and compares the results to those of previous slot-injection tests. In addition to short-duration schlieren and shadowgraph photography, concentration, pitot, cone-static, and stagnation temperature measurements are presented to document the development of the mixing layer. As anticipated, slot injection shows poor initial penetration of the injectant into the freestream, and therefore poor initial mixing. Nevertheless, the helium case shows better mixing than a similar air-injection case of a previous experiment; the mixing layer grows 25% larger than that in the air case by the last streamwise station. Also, about 30% more freestream air is entrained into the shear layer in the helium case and is confined mainly to the top third of the mixing layer. The higher mixing rate stems from larger gradients in velocity and density and lower mass-flux ratio values that result in greater turbulent transport in the helium-injection test. Measurements of organized structure angles and integral length scales are obtained using a parallel-array, dual-wire probe. Experimental results indicate the existence of organized structures in both the helium-injected and air-injected shear layers. The orientation of the measured angles is found to correlate with the local slope of the velocity profile. The integral length scale is on the order of 4 mm for both cases.

Nomenclature

A = area
a = constant in Eq. (1)
b = constant in Eq. (1)
d = hot-film diameter
f = function
H = slot height
k = thermal conductivity
ℓ = wire length
M = Mach number
m = constant in Eq. (1)
P = pressure
R = resistance
R_S = resistance in series with hot-film sensor in Wheatstone bridge
$\mathcal{R}$ = gas constant
T = temperature
U = streamwise velocity
V = voltage
w = wire separation distance
x = streamwise direction
y = vertical direction
α = mass fraction
γ = specific heat ratio
δ = boundary-layer thickness
θ = average structure angle
μ = fluid viscosity
ρ = density
τ = time delay
χ = mole fraction

Subscripts

c = sensor-plane channel
conv = convective
He = helium or helium-side
j = injectant or wall jet
max = maximum
s = static
t = total/stagnation
w = hot film
$*$ = throat
∞ = air freestream
2 = after normal shock

Presented as Paper 90-0093 at the AIAA 28th Aerospace Sciences Meeting, Reno NV, Jan. 8-11, 1990; received Feb. 5, 1990; revision received and accepted for publication Aug. 17, 1990.

*Graduate Assistant, Department of Aerospace and Ocean Engineering. Student Member AIAA.
†Graduate Assistant, Department of Mechanical Engineering.
‡Professor, Department of Mechanical Engineering. Senior Member AIAA.
§W. Martin Johnson Professor and Department Head, Department of Aerospace and Ocean Engineering. Fellow AIAA.

Introduction

WITH increased interest in supersonic and hypersonic atmospheric flight, considerable research is needed to investigate all aspects of developing vehicles that operate in this flow regime.[1] One main concern is the combustion dynamics involved in the supersonic combustion ramjets (SCRAMjets) that propel these vehicles. Inherently, mixing at high Mach numbers is relatively low. Moreover, at hypersonic flight Mach numbers of 8 to 20, the combustor Mach number remains supersonic. With such high velocities and low residence times, fuel must mix with air and burn quickly to prevent the need for excessively long combustors.[2] Therefore, the investigation of turbulent mixing qualities in this speed regime and various ways to augment mixing is essential.

Many fuel injection schemes are possible, each having its own advantages and disadvantages.[2-5] This study investigates the turbulent mixing layer resulting from supersonic tangential injection through a two-dimensional slot into a supersonic airstream. When the two parallel streams interact, a shear layer forms, trailing off the splitter-plate lip. This slot-injection flowfield is also characterized by expansions and shocks that propagate from the lip. The freestream boundary layer "rides" along the top of the shear layer until the shear layer spreads and engulfs both the external boundary layer and the injectant core.

Slot injection has several advantages. First, since the fuel injects parallel to the main flow, the momentum of the fuel adds to the total thrust produced by the engine. Second, tangential injection creates minimum disturbances within the

combustor. With fewer shocks and perturbations, total pressure losses are minimized, thus increasing engine efficiency. Another possible advantage is film cooling, where the injected fuel acts as a protective layer between the high stagnation-temperature freestream and the combustor wall.[6-10] Other benefits include skin-friction reduction[11-12] and boundary-layer energization, which discourages separation. Finally, because two-dimensional slot injection is a relatively simple case in terms of overall features, it acts as an appropriate baseline whereby the effectiveness of other configurations can be measured. The main disadvantage of slot flow is the lack of transverse penetration of the injectant, which promotes initial mixing, so that mixing rates are relatively low and spreading angles are small.

Another important motivation for experimental measurements is the inadequacies of most computational methods in predicting high-speed, turbulent, compressible flow. Even in the relatively simple case of slot injection, this holds true. Models based exclusively on free shear-layer aspects or boundary-layer qualities alone cannot fully represent the slot flowfield, since merging of a shear layer and a wall boundary layer exists. Turbulence modeling is complicated by merging viscous layers and the resulting presence of large gradients, especially in foreign gas injection. Although more current models attempt to address these deficiencies,[13,14] experimental measurements remain indispensable.

The literature contains numerous earlier studies of slot injection into a supersonic stream. These tests use various initial conditions, configurations, and techniques and investigate different aspects of slot injection.[6,9-12,15-17] However, the vast majority of these past experiments do not provide great detail in measuring the complete flowfield character. Some recent air injection tests with the same slot configuration and external flow as in this investigation[18,19] present a more thorough examination of the flowfield. This study results from a local progression along the same test matrix. The new parameter here is the use of helium instead of air as the injectant.

This paper begins with a description of the experimental background and techniques. Results are then presented for the supersonic slot injected flowfield at four downstream stations. Reduced data showing mean profiles of helium concentration, pitot pressure, Mach number, velocity, density, and mass flux are presented. In addition, results from measurements using a dual hot-wire probe are presented in terms of average organized structure angle and integral length scale of turbulence. Comparison of the changes in the flowfield characteristics between the previous air-injection test case and the present helium-injection test case is made.

Experimental Procedure

Facilities

The data for this study are obtained in the 23×23 cm blowdown supersonic wind tunnel at Virginia Tech. This tunnel provides run times of about 10 s at a freestream Mach number of 3.0, a total pressure of 6.5 atm, and a total temperature of 282 K. The resulting freestream unit Reynolds number is 5.4×10^5 per cm. The test section is 11.4-cm high, 22.8-cm wide, and more than 30-cm long in the streamwise direction. These dimensions are comparable to an actual SCRAMjet combustor.

The wind tunnel is computer operated and controlled, resulting in accurate and repeatable runs. The total pressure ($P_{t\infty}$) is maintained at ± 0.03 atm from run to run. The computer system also controls a 12-bit A/D data-acquisition system to sample and record various test parameters.

Slot Model

The slot injection model is built into the wind tunnel nozzle as shown in Fig. 1. The tangential-injection configuration consists of a 1.21-cm-high, downstream-facing slot separated from the Mach 3.0 mainstream by a splitter plate 0.5-mm thick. The slot height approximated the thickness of the freestream boundary layer at this location along the tunnel. The incoming boundary layer on the air side is developed along the wall of the lower nozzle block. Its pressure gradient history is governed by the pressure distribution along the nozzle block. Measurements made using a hot-wire probe have shown that the incoming boundary layer is turbulent. The contoured, converging-diverging injector has an area ratio of 1.55, and helium is injected at the total pressure of 0.89 atm. The nominal slot Mach number is 1.78. The exit static pressure ratio (P_j/P_∞) is 0.838, which matches that of the previous tests involving air slot injection. This allows a comparison to be made between the helium-air flowfield and the earlier air-air results.

Profiles across the shear layer are measured at four streamwise locations. Stations 1, 2, 3, and 4 correspond to x/H of 0.3, 4.1, 10.5, and 21.1, respectively.

Measurements of Mean Concentration

Accurate species concentration measurements for dissimilar gases are imperative to obtain accurate calculations of all mean-flow quantities. Many past experiments have measured species concentration using a sampling probe. Intrusive sampling requires an isokinetic condition. This is insured for supersonic flow if the standoff shock of the sampling probe is swallowed. If the shock is not swallowed, the standoff shock will deflect the lighter gas more than the air, resulting in a reading of lower concentration than is actually present.

To achieve the accurate species concentration sampling needed for this study, an aspirating hot-film probe was developed by Ng et al.[20] to measure local mean gas composition in supersonic flows. The geometry of the concentration probe and the cap design can be seen in Fig. 2. The sensor is a hot film with a diameter of 0.0508 mm (0.002 in.) and an active sensor length of 1.016 mm (0.040 in.). The hole inlet of the probe has a diameter of 0.279 mm (0.011 in.) and the choked orifice inside the probe has a diameter of 0.559 mm (0.022 in.). These dimensions are chosen to ensure the swallowing of the standoff shock. The swallowing of the shock has been verified by schlieren photographs taken of the probe tip during nominal operating conditions of the tunnel.

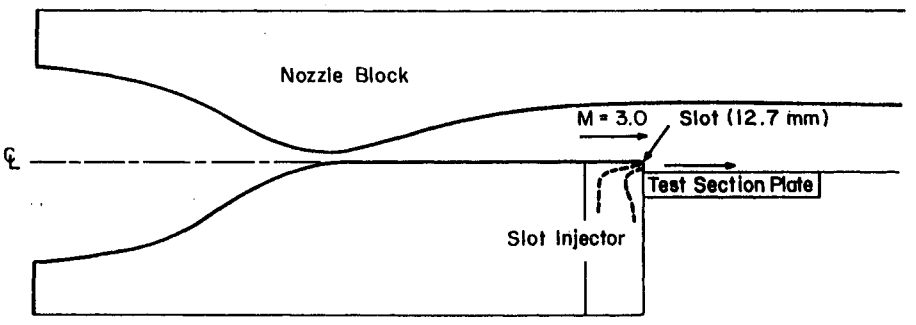

Fig. 1 Schematic of the wind-tunnel arrangement.

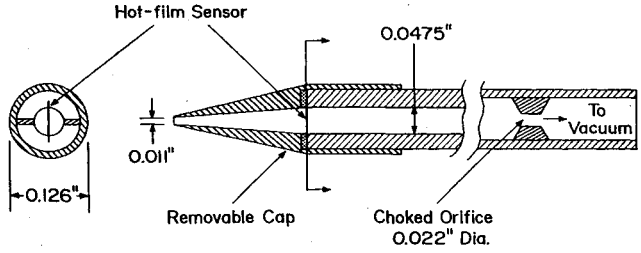

Fig. 2 Aspirating concentration probe geometry.

The governing equation for a hot film at constant temperature in a channel choked-exit is as follows:

$$V^2 = \frac{(R_s + R_w)^2}{R_w}\pi\ell k\left\{a\left[\frac{d}{\mu}\frac{P_t}{\sqrt{T_t}}\frac{A^*}{A_c}\sqrt{\frac{\gamma}{\Re}} \times \left(\frac{2}{\gamma+1}\right)^{\frac{\gamma+1}{2(\gamma-1)}}\right]^m + b\right\}(T_w - T_t) \quad (1)$$

This can be rewritten as $V^2 = f(\text{gas composition}, T_t, P_t)$, since k, γ, μ, and $\Re$ are functions of gas composition. Therefore, in order to determine gas composition, total pressure and total temperature profiles are needed. Details of the operation and calibration of the aspirating concentration probe can be found in Ref. 20.

Measurements of Other Mean Flow Quantities

Measurements of pitot pressure, cone-static pressure, and total temperature are made by traversing the shear layer at each of the four streamwise locations. The cone-static probe consists of a 10-deg semivertex-angle cone with a base diameter of 1.6 mm. A ceramic-tipped, vented, diffuser-type thermocouple probe is used to measure the total temperature. The sampling area of the probes is about 1×1 mm.

To reduce the raw data measured from a pitot probe and a cone-static probe, the concentration profile must be known to determine the gas constant and the ratio of specific heats. This information is then used in the Rayleigh pitot formula and the cone-flow solution in order to determine the Mach number and the static pressure in the flowfield from the measurements of the pitot and cone-static probe. Together with the measurements from the total measurement probe, all of the mean flow quantities such as velocity, density, and mass flux can be calculated.

Measurements of Large-Scale Structure Angle

One of the experimental objectives is to determine if organized structures exist in the flowfield and, if so, the corresponding structure angles. The measurements of structure angle in supersonic shear layers were first obtained by Robinson[21] and Spina and Smits.[22] The present study is the first time such measurements are obtained in a mixing layer. Details on the present experimental technique can be found in Ref. 23. The probe consists of a parallel-array, dual-wire probe with a fixed separation distance between hot wires of 1.33 mm (10% of the slot height). The hot wires are made of platinum-plated tungsten wires of 5-μm diam and 1.25-mm length. The dual-wire probe is connected to two separate constant temperature anemometers and operated at the same overheat ratio of 1.7.

For a given wire separation distance w, a structure passing the parallel wire probe at a given angle causes a time delay between the output of the hot wires. The time delay τ between the data resulting from the two hot-wire signals is obtained by performing a cross-correlation of the two signals. If this time delay is multiplied by the local mean velocity U, the structure angle associated with an average large-scale motion can then be calculated as follows:

$$\theta = \tan^{-1}\left[\frac{w}{U\tau}\right] \quad (2)$$

The angle θ may be called an "average structure angle," in that it is associated with an average large-scale motion. Strictly speaking, the local streamwise convection velocity should be used to determine this angle, but this convection velocity has not been determined for this flow. Although the local mean velocity is not necessarily equal to the convection velocity of the large scale motions, the difference in the mean structure angle owing to slight variations in the convection velocity is small, and therefore the average velocity is used here.

Measurements of Integral Length Scale

The hot-wire data used to determine the structure angles are also analyzed to determine the integral length scale of turbulence. The auto-correlation function of the hot-wire signal is calculated and integrated in time to provide the integral time scale. Using Taylor's hypothesis, if the integral time scale is multiplied by the local mean velocity, a characteristic length scale of turbulence is obtained. However, to the limit of the frequency response of the anemometer, turbulence length scales *less* than 3 mm cannot be resolved. Thus, all the length scale data presented in this paper are limited to 3 mm, even though the flowfield may contain length scales that are of smaller size. Details on the experimental technique to determine the integral length scale of turbulence can be found in Ref. 23.

Experimental Results

Flow Visualization

Spark-schlieren photographs (10^{-6} s) of the helium slot-injection into freestream air are presented in Fig. 3a. The flow moves from left to right, and the slot is located at the lower left corner. The air-side boundary layer before the injection station can be easily identified. The flowfield consists of the slot-injection boundary layer near the floor of the test section, the slot-injection freestream, a mixing region, and the tunnel freestream. The photograph also shows that the injected flow is slightly overexpanded. The adjustment shock and its reflection in the injectant stream are visible just downstream of the slot. The "lip" shock characteristic of base flows can be seen propagating up into the freestream.

The initial separation line (or dividing streamline) between the airstream and the helium flow shows up as a sharp white line from the lip of the splitter plate. This line corresponds to the maximum density gradient, and it remains clearly defined until station 2. Because P_j is less than P_∞, the separation line deflects toward the floor initially.

The development of the boundary layer at the tunnel floor is also clearly visible. Station 1 includes many waves in both the slot and the mainstream boundary layer. The potential core of the helium injection appears as the darker region below the mixing layer and above the lower wall boundary layer. Some mixing occurs by station 3, but the slot potential core still remains. From Fig. 3a, this core appears to extend to about $x/H = 15$. It should be pointed out that this provides only a rough estimate of the core length, because this dark feature depends on the lighting and arrangement of the optical equipment. At station 4, most of the potential core slot flow has decayed, and a substantially developed wall layer has formed, i.e., the shear layer and the lower-wall boundary layer appear to have merged together.

A nanoshadowgraph (10^{-9} s) picture of the same flowfield is presented in Fig. 4a. In a shadowgraph, fast varying gradients are highlighted, so that eddies and fluctuations become clearer as compared to the schlieren. High-frequency structures appear in the shear layer between stations 3 and 4. These

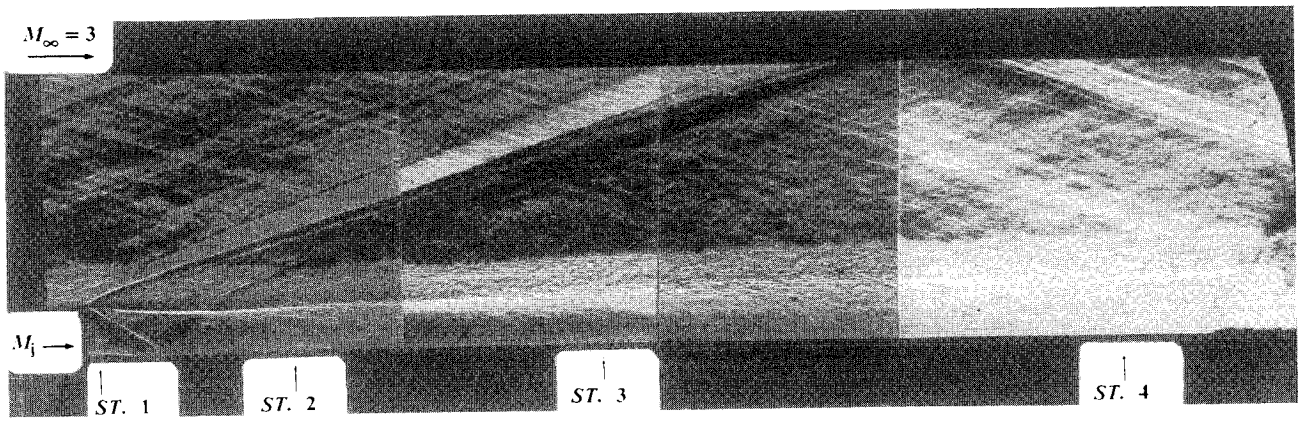

Fig. 3a Spark (10^{-6} s) schlieren of helium slot injection into an airstream.

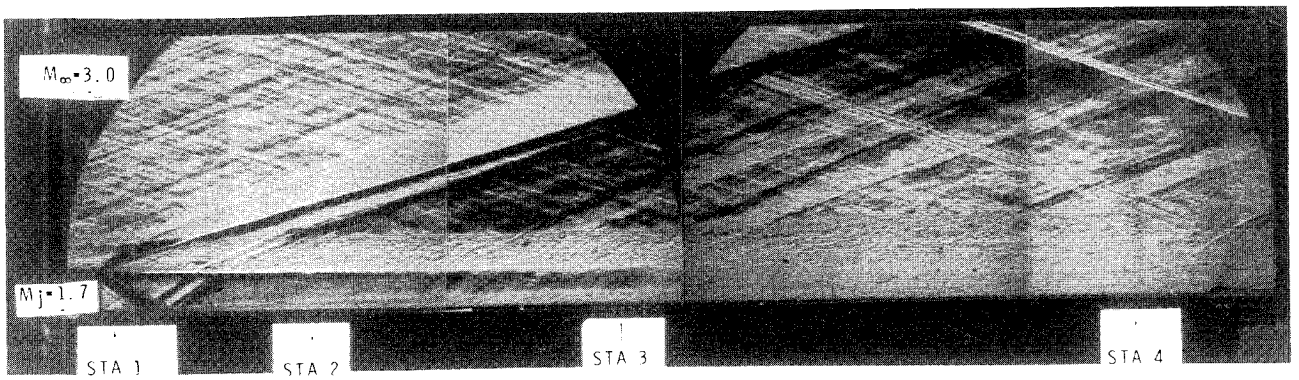

Fig. 3b Spark (10^{-6} s) schlieren of air slot injection into an airstream.[19]

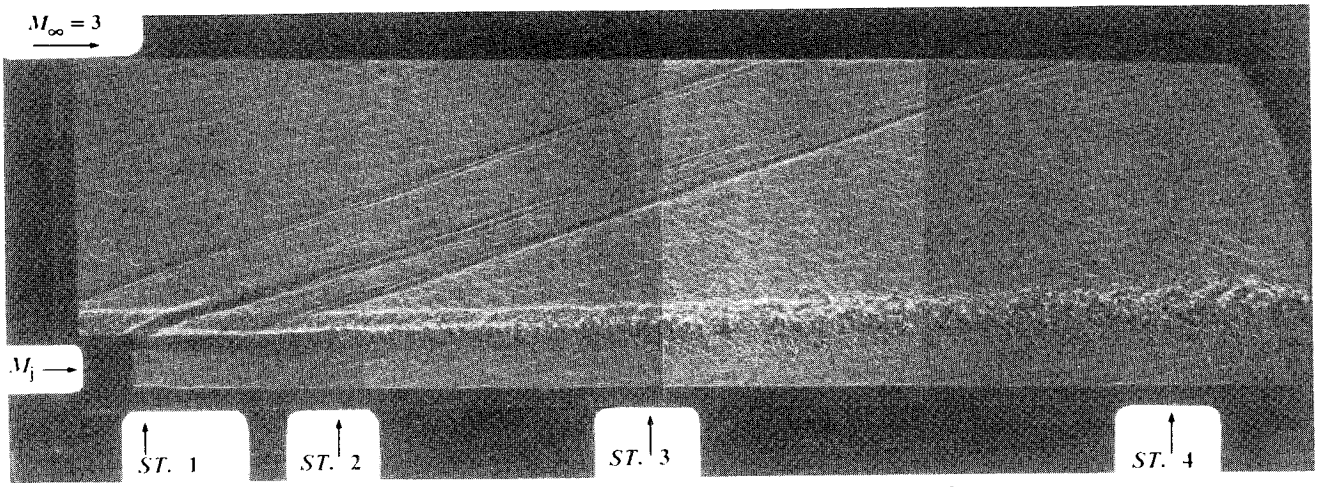

Fig. 4a Nano (10^{-9} s) shadowgraph of helium slot injection into an airstream.

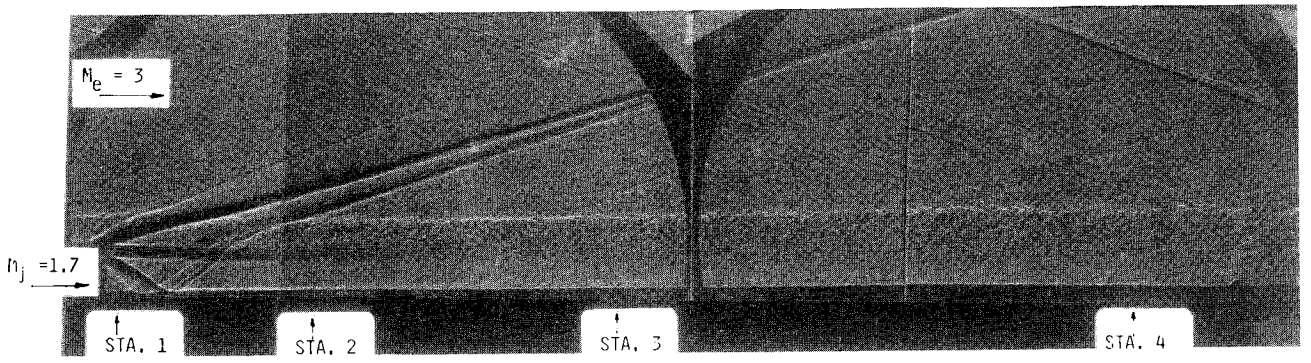

Fig. 4b Nano (10^{-9} s) shadowgraph of air slot injection into an airstream.[19]

large-scale structures are mainly restricted to the top of the shear layer. Underneath the structures, at the air-helium mixing boundary, finer fluctuations can be identified. With these small structures encroaching into the potential core of the injectant, the presence of turbulence is quite evident. Near station 1, the thickness of the boundary layer above the splitter plate is about 0.7 cm. This agrees with the velocity profile to be presented later. Initially, the dividing streamline separates the freestream boundary and the helium core, but by station 4, the shear layer completely engulfs the freestream boundary layer, so that an intermingled, fully turbulent region exists.

Flow Visualization—Comparison with Air Injection

Spark-schlieren photographs of air slot injection into freestream air are presented in Fig. 3b. From the two spark-schlieren photographs of Fig. 3, the full shear-layer region, characterized by the lightly shaded area as compared to the darker freestream region, grows 15% larger in the helium-injection case by station 4. This observation already indicates that with the helium injection the shear layer grows faster, signifying better mixing.

A nanoshadowgraph picture of the air slot injection into freestream air is presented in Fig. 4b. In comparing the two nanoshadowgraphs of Fig. 4, the most noticeable difference is the appearance of structures of two different scales in the helium-injection case. As already mentioned, near station 4, the helium-injection case shows larger structures at the upper edge of the shear layer, with smaller and finer structures appearing immediately below that. In the air-injection case, the organized structures appear to be of more uniform size.

Figures 3 and 4 also show that the shock structures found in the air and helium-injection cases are essentially identical. This is not surprising since the exit static pressure ratio of the helium injection case matches that of the air-injection case.

Concentration Profiles

Figure 5 shows the concentration profiles in terms of molar concentration. The decay of the slot flow due to mixing of the two steams is apparent. The profile at station 1 essentially shows a step change. Above $y/H = 1.00$, molar concentration goes to 0.0 as expected. At station 2, molar concentration is near 1.00 up to $y/H = 0.65$, and then the composition drops off to about 0.0 at $y/H = 1.10$. At stations 3 and 4, molar concentration drops below 1.00 throughout the entire profile, indicating some degree of mixing in the whole region. At station 3, helium concentration decreases near the wall. This is an unexpected occurrence.

Figure 6 shows the spreading rate of helium into the freestream air flow. The plot is obtained by defining the boundary of the mixing zone to be at the y/H location where the molar concentration of helium is 0.02, the resolution of the concentration probe. Figure 6 indicates that at station 4, the size of the mixing zone grows to about 2.1 slot heights. This result shows that the mixing shear layer spreads more rapidly than the flow visualization indicates; of course, measurements from the photographs are subject to greater uncertainty so that the mixing zone size from the concentration data is regarded as more accurate.

A complementary analysis technique to characterize the spreading rate of the injected fluid involves the "reaction-thickness" concept. The reaction thickness defines the vertical extent of the flowfield where the constituents are capable of sustaining a reaction. The lowest fuel concentration level capable of sustaining a reaction is termed the "fuel-lean" level and the maximum permissible concentration is called the "fuel-rich" level. The effective stoichiometric combustion ratio for hydrogen is a molar fuel concentration of 30%. However, the concentration range wherein combustion may take place is much larger. For hydrogen/air, the reaction thickness corresponds to regions of the flow where the mole fraction of

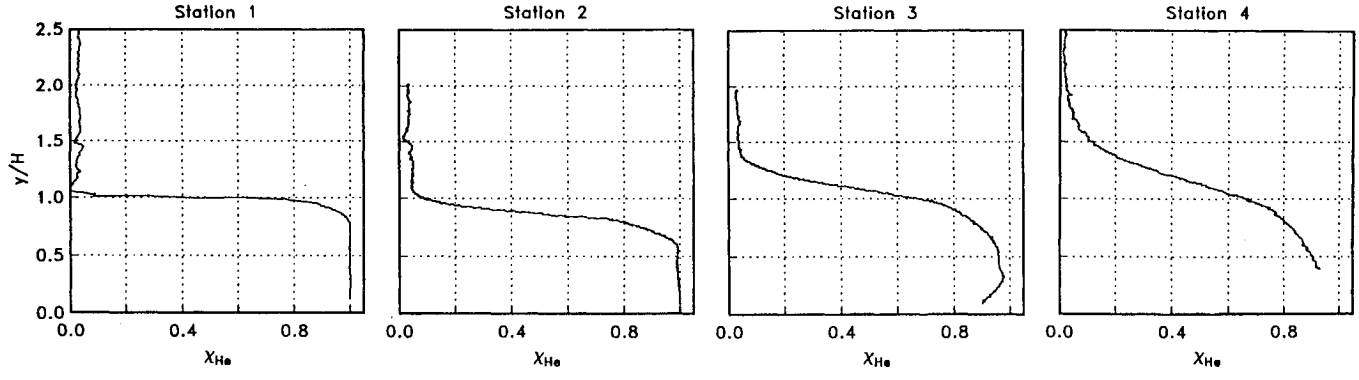

Fig. 5 Molar concentration profiles.

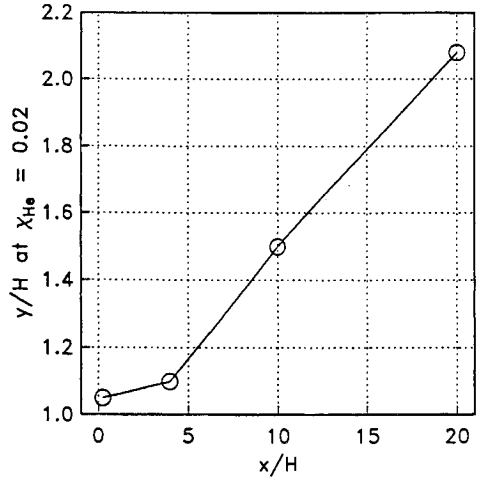

Fig. 6 Spreading rate of mixing layer.

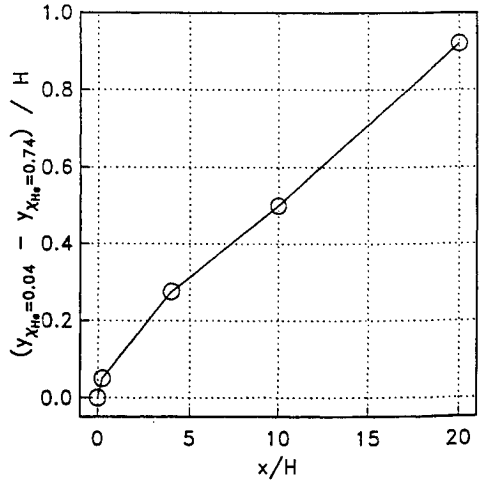

Fig. 7 Reaction layer thickness.

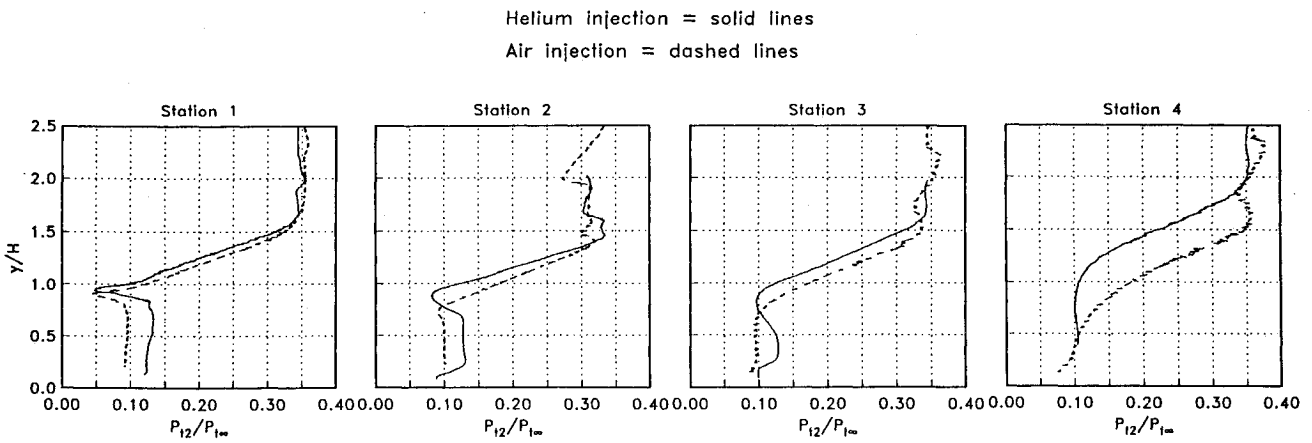

Fig. 8 Comparison of pitot pressure profiles.

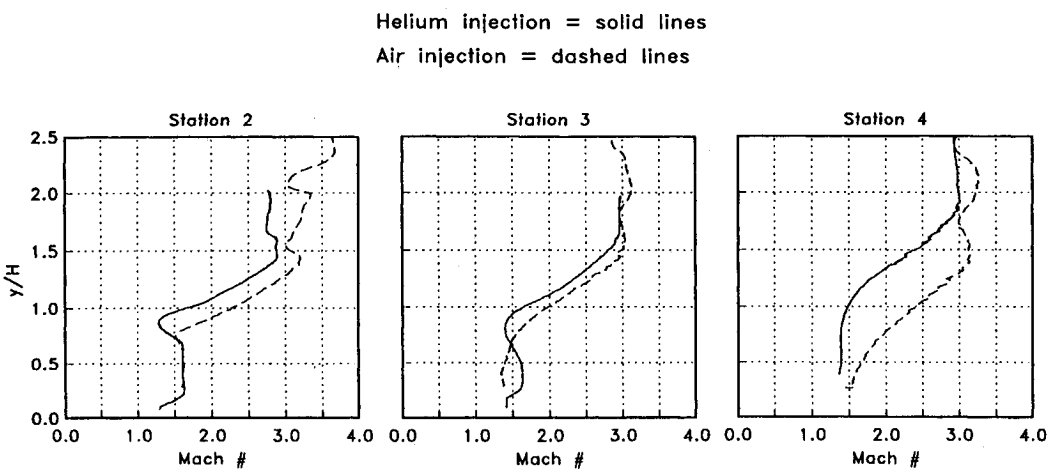

Fig. 9 Comparison of Mach number profiles.

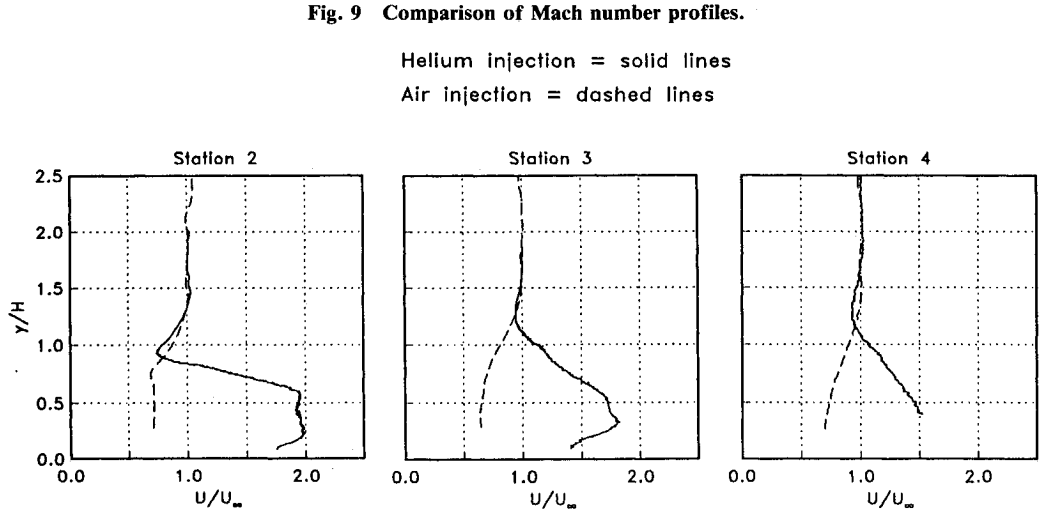

Fig. 10 Comparison of velocity profiles.

hydrogen is between 0.04 and 0.74. If we assume helium "fuel" behaves in the same way as hydrogen, the concentration data of Fig. 5 may be used to obtain the reaction thickness. The results are shown in Fig. 7. It can be seen that the reaction thickness increases linearly as a function of downstream distance and, at station 4, the normalized reaction thickness has grown to 0.95 slot height.

Mean Flow Profiles

The complete set of mean flow profiles consist of both helium- and air-injection cases for comparison. Each profile is normalized using its corresponding freestream value.

Figure 8 shows the data from the pitot probe for both the helium- and air-injection cases. The trends are generally well behaved and as expected. For the most part, the magnitudes and trends are comparable, since external stream test conditions are matched. At station 4, the pitot pressure P_{t2} smoothes out at $y/H = 2.0$ for helium and $y/H = 1.5$ for air. The wake region due to the splitter plate for the helium case is larger and slightly higher as shown at stations 1, 2, and 3 in Fig. 8. Figure 9 gives the Mach number profiles for both cases, calculated from the cone static and pitot pressures. The cone-static probe is very sensitive to impinging waves on the tip. Because of the adjustment shock emanating from the injector

and impacting on the cone tip, data taken at station 1 are suspect and, hence, are not presented. At station 2, both helium- and air-slot Mach number profiles are uniform, since there are no waves present to distort the flow. The dip from the wake occurs below $y/H = 1.0$ due to the downward curvature of the separation line. At this station, both cases show the freestream Mach number varying about 3.0 above $y/H = 1.4$. This is due to the complex wave pattern in the freestream in this region. By station 4, both cases show that the slot flow has completely blended in with the splitter plate wake, so that they cannot be distinguished.

Figure 10 shows the two velocity distributions normalized by their respective freestream velocities. At station 2, the maximum helium injection velocity is 1.8 times the freestream velocity, while the air injection has a velocity 0.7 times the freestream value. The maximum ratio of the helium-injection velocity to freestream velocity decays to 1.7 and 1.5 at stations 3 and 4. The higher slot velocity compared to the freestream is due to the low molecular weight of helium. With the velocity gradient $\partial U/\partial y$ greater for the helium case, better mixing is anticipated.

Figure 11 documents the density distributions. At station 2, the helium density is about 0.1 of the freestream air density. This density ratio remains relatively unchanged even at stations 3 and 4. For the air injection, the density ratio of the slot flow to the freestream air is about 0.6 for all stations.

Figure 12 combines the density and velocity effects into a single term ρU, the mass flux. In general, $\rho U/\rho_\infty U_\infty$ values further away from unity promote mixing,[16] and the comparison between helium injection and air injection supports this idea. The $\rho U/\rho_\infty U_\infty$ for helium gives a good estimate of the mixing-layer thickness. In the helium-injection case, the concentration profiles directly indicate the mixing-zone size at each station. Unfortunately, with the air-injection case, there

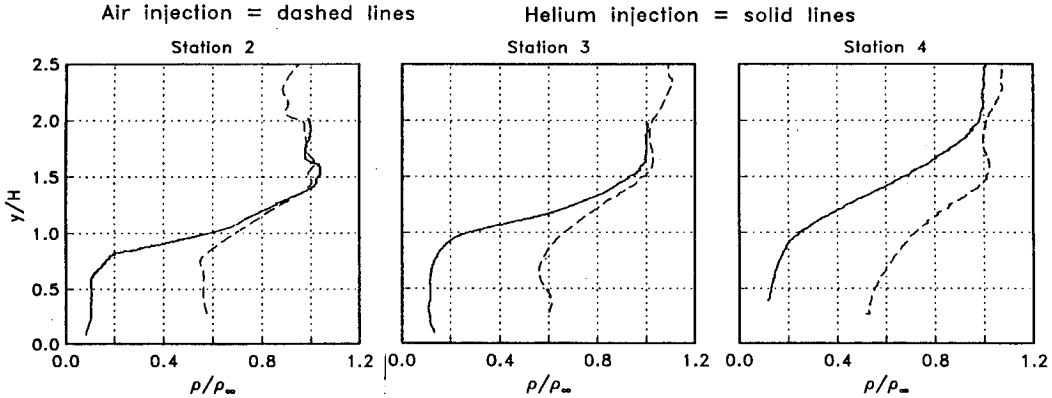

Fig. 11 Comparison of density profiles.

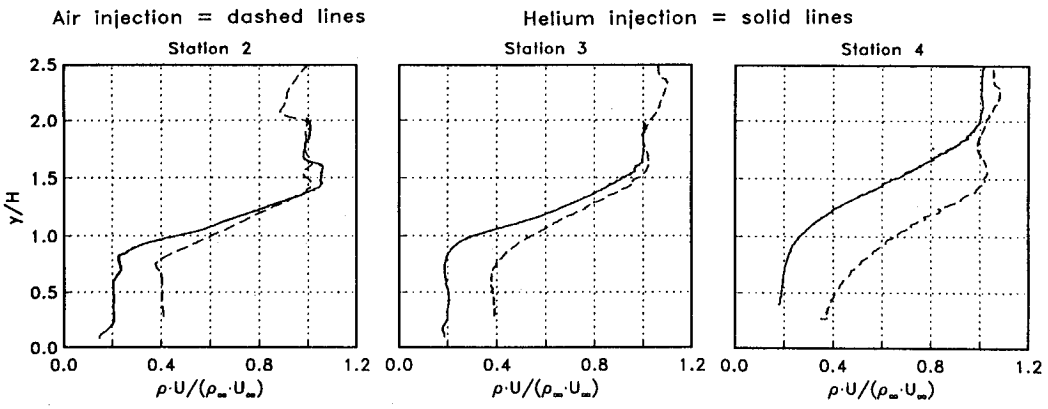

Fig. 12 Comparison of mass-flux profiles.

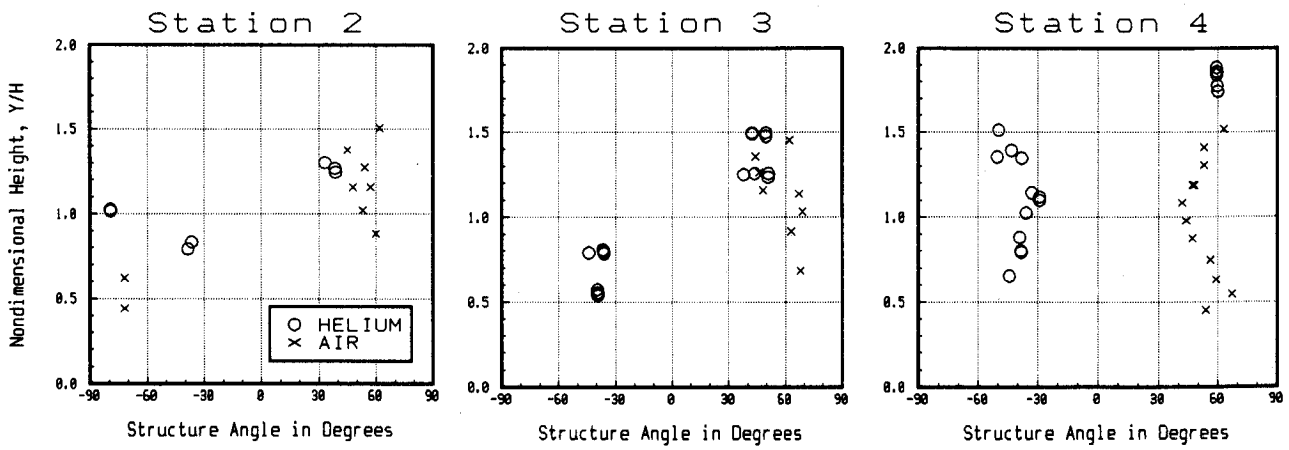

Fig. 13 Comparison of large-scale structure angle.

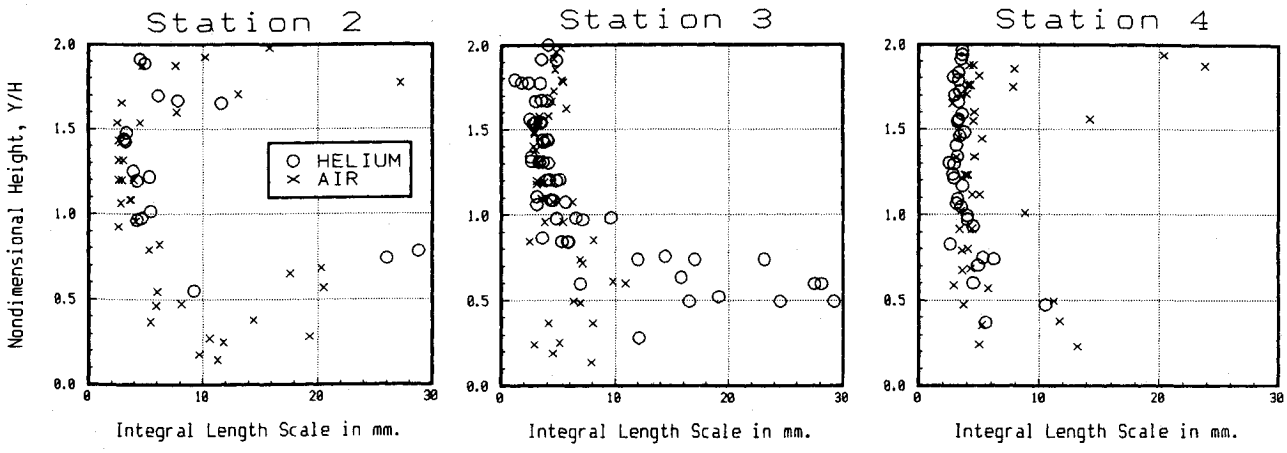

Fig. 14 Comparison of integral length scale.

is no corresponding measurement. By comparing the trends in station 4 of the ρU and concentration profiles for helium injection, however, ρU can be seen to reach a constant value at about the same point as the concentration goes to where $\chi_{He} = 0.0$. Therefore, by this observation, ρU is found to be a good indicator of the mixing-layer height in this slot-injection configuration. For the air-injection case then, if ρU is assumed to indicate mixing-layer size, the nondimensional mixing-layer thickness at station 4 is about 1.6 from the ρU profile. Thus, the helium case, with a normalized mixing-layer thickness of 2.1, shows 25% more growth in the mixing layer by station 4.

Large-Scale Structure Angle

In Ref. 21, results from the measurements of the large-scale structure angle in the air-injection case are presented and discussed in detail. Results of the measurements for the average structure angle for both air- and helium-injection cases are presented in Fig. 13 for comparison. Positive and negative angles are defined as counterclockwise and clockwise rotations, respectively, from a horizontal axis. At station 2 for the case of helium injection, the average structure angles are observed to be -38 deg in the lower portion of the shear layer, decreasing to about -80 deg at y/H just over 1. Above y/H of 1.2, the structure angles are about 37 deg. Figure 13 for station 2 shows that an abrupt transition occurs in the calculated average structure angles for both air and helium injection. In both cases, the average structure angles are negative in the lower region of the shear layer and positive in the upper region. The existence of a negative structure angle is thought to be attributable to the presence of an "inverted boundary-layer" profile. For example, inspection of Fig. 10 at station 2 for y/H between 0.6 and 0.9 reveals that the helium velocity profile is inverted relative to the familiar boundary-layer profile. Above y/H of 0.9, Fig. 10 shows a helium velocity profile similar in shape to conventional boundary layers. This is consistent with the observation of positive structure angles in Fig. 13 at station 2 for $y/H > 1.2$. This region above $y/H = 0.9$ is dominated by the boundary layer developed upstream of injection.

For the case of air injection at station 2, the distribution of average structure angle is also consistent with the velocity profile shown in Fig. 10. Upon close inspection of Fig. 10 below $y/H = 0.75$, the "inverted boundary-layer" profile that results in the negative structure angle of about -72 deg is apparent. Above y/H of 0.7 is the conventional boundary-layer profile, resulting in an average structure angle of 50 deg.

At station 3, the helium velocity in Fig. 10 is again "inverted" in the region $y/H = 0.5$ and 1.2. In this region, the average structure angles are between -36 and -44 deg. Above $y/H = 1.2$, the average structure angles lie between 30 and 51 deg. Thus, the average structure angles for the helium-injection case at stations 2 and 3 follow similar trends with respect to the velocity profile.

From the velocity profile for the air injection at station 3 in Fig. 10, a region dominated by the upstream boundary layer remains clearly visible between $y/H = 0.7$ and 1.5. The large-scale structure for this case follows a similar trend as the velocity profile in that the angles are all positive, with a mean of about 60 deg. The negative structure angle at station 2 is not observed and this is consistent with the absence of the inverted boundary layer at this station. In summary, the large-scale structure angles presented in Fig. 13 for station 3 follow a similar trend as the velocity profiles both air and helium injections.

Results at station 4 are also presented in Fig. 13. For air injection, the velocity profile in Fig. 10 begins to take on more of the appearance of a single boundary layer. A mean structure angle of 56 deg can be seen in Fig. 13, which is in general agreement with the mean angle at station 3. For helium injection, the velocity profile in Fig. 10 indicates that between y/H of 0.4 and 1.2, the flowfield is dominated by the inverted boundary layer velocity profile. The corresponding structure angle in this region is about -40 deg. Above y/H of 1.2, the velocity profile is similar to that of a conventional boundary layer, and the corresponding structure angle in this region is about 60 deg.

Integral Length Scale

Results for the integral length scale are summarized in Fig. 14. At station 2, above the wake of the splitter plate ($y/H > 0.8$), the characteristic length scale for the air injection is about 3 mm. The length scale for the helium injection in the same region is about 4 mm. At this station, the lower portion of the flowfield ($y/H < 0.8$) shows integral length scales that scatter around 5 to 20 mm for air injection. For helium injection, the maximum length scale in this region is as much as 30 mm. This region represents the freestream of the slot, and the intermittency at the lower edge of the shear layer and at the edge of the lower-wall boundary layer may account for the variation in length scale.

At station 3, the region above y/H of 1.0 remains unchanged compared to station 2. The integral length scale for air injection is relatively uniform and centers around 3 mm. For helium injection the length scale appears to be slightly higher. For air injection the lower portion of the flowfield ($y/H < 1.0$) experiences some modification; the variation in the length scale is now between 5 and 30 mm. These data suggest that there is a change in the turbulence structure between stations 2 and 3 in the slot region for the air injection, whereas no measurable change is observed for the helium injection.

At the last survey station, the overall distribution of the integral length scale changes considerably for both cases. The

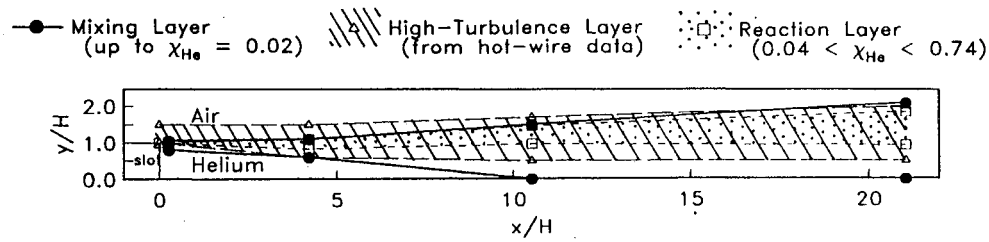

Fig. 15 Characteristic layers of the flowfield.

scatter in the lower portion of the shear layer is reduced, with very few data points showing a length scale of 5 mm or more. For the upper portion of the shear layer ($y/H > 1.0$), helium injection shows a length scale of about 3 mm at station 4. In this upper portion of the shear layer, it appears that there is a slight reduction in length scale for the helium injection between station 2 and station 4. On the contrary, air-injection data show a slight increase in the same region of the flowfield. It should be pointed out that the measurements of the integral length scale are very close to the resolution limit (3 mm) of the measurement technique. This makes it difficult to draw any significant conclusions from the data.

Discussion

A further basis for comparison of the helium and air injection is the entrainment rate of freestream air into the viscous layer. The entrainment rate is quantified by calculating the difference in mass flow rate between stations 1 and 4, thus giving the amount of freestream air entrained by station 4. The mass flow rate at each station is calculated by numerically integrating the mass flux profiles. Results show that the helium-injection case entrains 30% more freestream air into the shear layer than the air-injection case. As an overall consistency check for the helium case, the mass flow rate of helium at station 4 is deduced and compared to the mass flow rate of helium at station 1. The values are found to agree within the experimental error of the concentration measurement (±2% mole fraction helium).

By changing the upper limit of integration of the mass flux at station 4 for the helium case, most of the entrainment of air is found to occur along the top third of the mixing layer. This result codifies the observation that, though the helium shear layer grows faster, the helium core seems more pronounced at station 4 than the core for the air-injection case. In other words, although there is air mixed into the entire region up to the wall, a significant core can still exist if most of the interaction is confined to the upper portion of the shear layer. This phenomenon is more pronounced in the helium-injection case. This feature further suggests that the majority of the mixing occurs along the two-gas interface within the large-scale eddies of the shear layer and that lower-level, almost secondary, mixing occurs within the wall region. In short, there seems to be two regions of mixing: an "active" area at the interface between the two constituents in the shear layer and a relatively "passive" zone below the shear layer.

Figure 15 summarizes the characteristic layers in the helium slot-injection flowfield. The mixing layer is defined as the region in the flowfield where the helium molar concentration, χ_{He}, is between 0.0 and 1.0. The high-turbulence layer is obtained from the hot-wire data as well as the shadowgraph photos. The plot also includes the reaction layer, which, again, is defined as the region where the molar concentration of helium is between 0.04 and 0.74.

An independent parameter that may shed more light on mixing comparisons between air- and helium-injection cases is the convective Mach number introduced by Bogdanoff[24] and used by others.[25-27] Their argument states that, for compressibility effects in supersonic shear flows, the Mach number relative to a coordinate frame moving with the large-scale structures strongly influences mixing properties, not the "laboratory" Mach number relative to a fixed coordinate system. Moreover, an imporant trend is that, as the convective Mach number M_{conv} increases toward unity, mixing becomes poorer. Thus, with this model and its related formulas, M_{conv}, as calculated with the present initial conditions, is about 0.7 in the helium case and 0.3 for air injection. Accordingly, the air case should mix better than the helium case, based solely on compressibility effects. Helium injection, however, is found to mix better in the experiments. Thus, there seem to be other factors that may influence mixing, other than the convective Mach number compressibility factor alone. Velocity gradients may prove to have a greater influence in this region, since they are quite large in the helium case and have direct impact on vorticity production. In addition, the mass-flux ratio is smaller for the helium case, and as has been previously stated, lower ρU values enhance mixing. This contribution may be greater than what the M_{conv} model accounts for. Moreover, the convective Mach number model concentrates on free shear layers, whereas in this study the shear layer is wall-bounded on one side. The merging viscous zones and possible resulting self-induced pressure gradients[28] may have an adverse effect on the applicability of this model. Also, another inherent assumption of the model is that a step change in flow quantities occurs across the lip of the splitter plate. In the actual test case, however, a sizable freestream boundary layer δ initially "rides" on top of the forming shear layer. Previous experimentation with this theory suggests that in this type of flowfield, the region where the complete M_{conv} similarity solutions apply does not occur until about $x = 25\delta$ downstream.[29] Thus, the furthest downstream stations of this study are located in the part of the flow where M_{conv} applicability just begins to have a larger influence. In the near-field, which this paper documents, gradients and ρU effects may play a more important role.

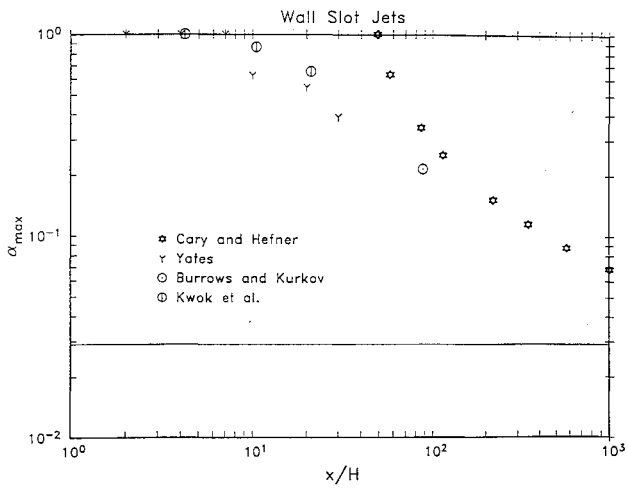

Fig. 16 Downstream decay of the maximum concentration for wall slot jets.[5]

To determine how well the data from this study fits in with other tests, mass fraction (α_{max}) decay data from various experiments involving slot injection into a supersonic airstream are presented in Fig. 16. This plot includes the present study as

well as investigations by Yates,[16] Burrows and Kurkov,[30] and Cary and Hefner[10] and shows α_{max} decay at several downstream locations. Yates injected hydrogen at $M_j = 1.2$ into a freestream at $M_\infty = 2.1$ and captured gas-composition information using a sampling probe. The data of Yates compare reasonably well with the present study, performed at roughly similar conditions. Investigating sonic hydrogen injection into a Mach 2.5 freestream, Burrows and Kurkov provide one concentration point at $x/H = 89$. Also, the experiments of Cary and Hefner indirectly give concentration levels at several locations beyond $x/H = 21$; the α_{max} is deduced from their data on wall effectiveness[5] of sonic slot-injection film cooling with air ($M_\infty = 6$). These last two data sets provide an indication of possible far-field mixing and α_{max} decay for the present helium slot-injection case.

Summary and Conclusions

This investigation represents a step toward detailing the flowfields of different injection schemes and providing more information on high-speed mixing dynamics. In particular, this study compares the helium slot injection to air slot injection at similar conditions in supersonic flow, which helps to provide more information on flow dynamics within the shear layer and the effect of different gases in similar test configurations. The mixing layer is 25% larger than that in the air-injection case. Also, 30% more freestream air is entrained into the shear layer. Interestingly, even though by station 3 some degree of mixing occurs throughout the shear layer/wall region, most of the total mixing is confined to an active zone in the top third of the mixing layer where gradients are largest and transport mechanisms are most energetic. This observation indicates that most of the mixing occurs in the high-turbulence layer while a smaller degree of mixing is present outside the turbulence layer but within the mixing layer. Results from the turbulence measurements using a dual-wire probe indicate the existence of organized structure in the flowfield. The integral length scale of turbulence is measured to be about 4 mm. Furthermore, for helium injection, both positive and negative angles are present, with an abrupt transition between the two groups. The structures in the air-injected shear layer have positive angles almost exclusively. The difference in orientation between the helium-injection and air-injection angles is attributable to the local slopes of their respective velocity profiles.

Acknowledgments

This work was supported by the Applied Physics Laboratory of the Johns Hopkins University, Harold E. Gilreath, Contract Monitor.

References

[1]Waltrup, P. J., "Liquid Fueled Supersonic Combustion Ramjets: A Research Perspective of the Past, Present and Future," AIAA Paper 86-0158, Jan. 1986.

[2]Mays, R. B., Thomas, R. H., and Schetz, J. A., "Low Angle Injection into a Supersonic Flow," AIAA Paper 89-2461, July 1989.

[3]Schetz, J. A., Weinraub, R. A., and Mahaffey, R. E., Jr., "Supersonic Transverse Injection into a Supersonic Stream," *AIAA Journal*, Vol. 6, No. 5, 1968, p. 934.

[4]King, P. S., Thomas, R. H., Schetz, J. A., and Billig, F. S., "Combined Tangential-Normal Injection into a Supersonic Flow," AIAA Paper 89-0622, Jan. 1989.

[5]Schetz, J. A., Thomas, R. H., and Billig, F. S., "Mixing of Transverse Jets and Wall Jets in Supersonic Flow," IUTAM Symposium on Separated Flows and Jets, Novosibirsk, USSR, July 1990.

[6]Goldstein, R. J., Eckert, E. R. G., Tsou, F. K., and Haji-Sheikh, A., "Film Cooling with Air and Helium Injection through a Rearward-Facing Slot into a Supersonic Air Flow," *AIAA Journal*, Vol. 4, No. 6, 1986, pp. 981–985.

[7]Goldstein, R. J., Rask, R. B., and Eckert, E. R. G., "Film Cooling with Helium Injection into an Incompressible Air Flow," *International Journal of Heat and Mass Transfer*, Vol. 9, No. 12, 1966, pp. 1341–1350.

[8]Stollery, J. L., and El-Ehwany, A. A. M., "Shorter Communication on the Use of a Boundary-Layer Model for Correlating Film Cooling Data," *International Journal of Heat and Mass Transfer*, Vol. 10, No. 1, 1967, pp. 101–105.

[9]Burns, W. K., and Stollery, J. L., "The Influence of Foreign Gas Injection and Slot Geometry on Film Cooling Effectiveness," *International Journal of Heat and Mass Transfer,* Vol. 12, No. 8, 1969, pp. 935–950.

[10]Cary, A. M., Jr., and Hefner, J. N., "Film Cooling Effectiveness in Hypersonic Turbulent Flow," *AIAA Journal*, Vol. 8, No. 11, 1970, pp. 2090–2091.

[11]Kenworthy, M., and Schetz, J. A., "Experimental Study of Slot Injection into a Supersonic Stream," *AIAA Journal*, Vol. 11, No. 5, 1973, pp. 585–586.

[12]Schetz, J. A., and vanOvereem, J., "Skin Friction Reduction by Injection Through Combinations of Slots and Porous Sections," *AIAA Journal*, Vol. 13, No. 8, 1975, pp. 971–972.

[13]Schetz, J. A., Billig, F. S., and Favin, S., "Simplified Analysis of Slot Injection in Hypersonic Flow," AIAA Paper 88-3056, July 1988.

[14]Situ, M., and Schetz, J. A., "New Mixing Length Model for Turbulent High-Speed Flows," AIAA Paper 89-1821, 1989.

[15]Visich, M., Jr., and Libby, P. A., "Experimental Investigation of Mixing of Mach Number 3.95 Stream in Presence of Wall," NASA TN D-247, Feb. 1960.

[16]Yates, C. L., "Two-Dimensional, Supersonic Mixing of Hydrogen and Air Near a Wall," NASA CR-1793, March 1971.

[17]Waltrup, P. J., and Schetz, J. A., "Tangential Slot Injection of Carbon Dioxide and Helium into a Supersonic Air Stream," ASME Paper 72-WA/FE-37, July 1972.

[18]Walker, D. A., Campbell, R. L., and Schetz, J. A., "Turbulence Measurements for Slot Injection in Supersonic Flow," AIAA Paper 88-0123, Jan. 1988.

[19]Hyde, C., Smith, B., Schetz, J., and Walker, D., "Turbulence Measurements for Heated Gas Slot Injection in Supersonic Flow," AIAA Paper 89-1868, June 1989.

[20]Ng, W. F., Kwok, F. T., and Ninneman, T. A., "A Concentration Probe for the Study of Mixing in Supersonic Shear Flows," AIAA Paper 89-2459, July 1989.

[21]Robinson, S. K., "Space-Time Correlation Measurements in a Compressible Turbulent Boundary Layer," AIAA Paper 86-1130, 1986.

[22]Spina, E. F., and Smits, A. J., "Organized Structures in a Compressible, Turbulent Boundary Layer," *Journal of Fluid Mechanics*, Vol. 182, No. 1, 1987, pp. 85–109.

[23]Clark, R. L., Ng, W. F., Walker, D. A., and Schetz, J. A., "Large-Scale Structure in a Supersonic Slot-Injected Flowfield," *AIAA Journal*, Vol. 28, No. 6, 1990, pp. 1045–1051.

[24]Bogdanoff, D. W., "Compressibility Effects in Turbulent Shear Layers," *AIAA Journal*, Vol. 21, No. 6, 1983, pp. 926–927.

[25]Papamoschou, D., and Roshko, A., "Observations of Supersonic Free Shear Layers," AIAA Paper 86-0162, Jan. 1986.

[26]Samimy, M., and Elliott, G. S., "Effects of Compressibility on the Structure of Free Shear Layers," AIAA Paper 88-33054A, July 1988.

[27]Samimy, M., Erwin, D. E., and Elliott, G. S., "Compressibility and Shock Wave Interaction Effects on Free Shear Layers," AIAA Paper 89-2460, July 1989.

[28]Ferri, A., "A Critical Review of Heterogeneous Mixing Problems," *Astronautica Acta*, Vol. 13, Nos. 5 and 6, 1968, pp. 453–465.

[29]Bushnell, D. M., private communication, 1990.

[30]Burrows, M. C., and Kurkov, A. P., "Supersonic Combustion of Hydrogren in a Vitiated Air Stream Using Stepped-Wall Injection," AIAA Paper 71-721, June 1971.